The Cryosphere
Discussions

Open Access

LiDAR snow cover studies on glacier surface: significance of snow- and ice dynamical processes

K. Helfricht[1,2], M. Kuhn[2], M. Keuschnig[1,3], and A. Heilig[4,5]

[1]alpS – Centre for Climate Change Adaptation, Grabenweg 68, 6020 Innsbruck, Austria
[2]Institute of Meteorology and Geophysics, University of Innsbruck, Innrain 52, 6020 Innsbruck, Austria
[3]Department of Geography and Geology, University of Salzburg, Hellbrunnerstrasse 34, 5020 Salzburg, Austria
[4]Commission for Geodesy and Glaciology, Bavarian Academy of Sciences and Humanities, Alfons-Goppel-Str. 11, 80539 Munich, Germany
[5]Institute of Environmental Physics, University of Heidelberg, Im Neuenheimer Feld 229, 69120 Heidelberg, Germany

Correspondence to: K. Helfricht (helfricht@alps-gmbh.com)

TCD

7, 1787–1832, 2013

LiDAR snow cover studies on glacier surface

K. Helfricht et al.

Title Page

Abstract	Introduction
Conclusions	References
Tables	Figures

◄	►
◄	►
Back	Close

Full Screen / Esc

Printer-friendly Version

Interactive Discussion

Abstract

The storage of water within the seasonal snow cover is a substantial source for runoff in high mountain catchments. Information about the spatial distribution of snow accumulation is necessary for calibration and validation of hydro-meteorological models.
5 Generally only a small number of precipitation measurements deliver precipitation input for modeling in remote mountain areas. The spatial interpolation and extrapolation of measurements of precipitation is still difficult. Multi-temporal application of Light Detecting And Ranging (LiDAR) techniques from aircraft, so-called airborne laser scanning (ALS), enables to derive surface elevations changes even in inaccessible terrain.
10 Within one snow accumulation season these surface elevation changes can be interpreted as snow depths as a first assumption for snow hydrological studies. However, dynamical processes in snow, firn and ice are contributing to surface elevation changes on glaciers. To evaluate the magnitude and significance of these processes on alpine glaciers in the present state, ALS derived surface elevation changes were compared
15 to converted snow depths from 35.4 km of ground penetrating radar (GPR) profiles on four glaciers in the high alpine region of Ötztal Alps. LANDSAT data were used to distinguish between firn and ice areas of the glaciers. In firn areas submerging ice flow and densification of firn and snow are contributing to a mean relative deviation of ALS surface elevation changes from actually observed snow depths of −20.0 % with a mean
20 standard deviation of 17.1 %. Deviations between ALS surface elevation changes and GPR snow depth are small along the profiles on the glacier tongues. At these areas mean absolute deviation of ALS surface elevation changes and GPR snow depth is 0.004 m with a mean standard deviation of 0.27 m. Emergence flow leads to distinct positive deviations only at the very front of the glacier tongues. Snow depths derived
25 from ALS deviate less from actually measured snow depths than expected errors of in-situ measurements of solid precipitation. Hence, ALS derived snow depths are an important data source for both, spatial distribution and total sum of the snow cover

volume stored on the investigated glaciers and in the corresponding high mountain catchments at the end of an accumulation season.

1 Introduction

In alpine mountain catchments the so-called glacio-nival runoff regime is caused by the storage of water in the seasonal snow cover and in glaciers (Aschwanden et al., 1986; Kuhn and Batlogg, 1998; Kuhn, 2000). Whereas winter runoff is reduced, enhanced runoff is generated by snow melt from unglacierized and glacierized areas at the beginning of the ablation season in spring. In the summer months melting of the snow cover at high elevation and ice ablation at the glaciers are the main resources of runoff. These enhanced flow rates in spring and summer are subject of interest in terms of water resources management, e.g. in water power production. Peak flow rates generated by heavy rainfall in combination with snow or ice melt are subject to flood forecasting (Schöber et al., 2012b).

The spatial distribution of snow accumulation is controlled by topography and atmospheric conditions in the mountain catchments. Distinct patterns of snow accumulation are produced by redistribution through wind,gravity and spatially differing melt processes (Bernhardt et al., 2008; Strasser, 2008; Dadic et al., 2010; Mott et al., 2010). Further complex relations exist between the glacier surface and the snow accumulation, and vice versa. Overall a redistribution of snow from unglacierized slopes towards glacier surface is observed and is a basic process for the existence of alpine glaciers (Kuhn, 2003).

The redistribution of snow has to be considered in hydro-meteorological models for calculating reliable glacier mass balances and runoff amounts. The spatial variability of the alpine snow cover can be simulated in an empirical process-based way (e.g. Lehning et al., 2006; Huss et al., 2008; Strasser, 2008) or described by statistical relationships between snow depth and topographic parameters (e.g. Baños et al., 2011; Schirmer et al., 2011). However, measured precipitation, which is used as input for

LiDAR snow cover studies on glacier surface

K. Helfricht et al.

modeling, is known to be affected by considerable errors. Especially rain gauge measurements of solid precipitation in high mountain environments underestimate the total precipitation volume to a significant proportion of up to 50 % (Sevruk, 1985). Only insufficient data are available for model calibration and validation in terms of snow depth distribution. Snow depth, snow density and snow water equivalent (SWE) can be derived from snow depth probing and snow pits (Fierz et al., 2009). Direct glacier mass balance measurements are a source for additional data in glacierized catchments. However, only on a small number of glaciers annual surface glacier mass balances are monitored worldwide (Zemp et al., 2009). Even on less glaciers summer mass balance and winter mass balance are treated separately. The inter- and extrapolation of the measured snow depths and snow densities need additional information itself (Escher-Vetter et al., 2009; Fischer, 2010). Likewise, automatic measurement systems for snow depth and snow density are operating on the point scale only (Lundberg et al., 2010). Various hydro-meteorological models have been tested versus information from extraterrestrial remote sensing products like MODIS or LANDSAT scenes for validating the areal snow cover extent (e.g. Hall et al., 2002; Schöber et al., 2010). To date no snow depth or SWE can be obtained from satellite data in a high spatial resolution of less than 100 m (Lundberg et al., 2010; Nolin, 2011).

Numerous applications of the upcoming technique of Light Detecting And Ranging (LiDAR) were recognized to be useful as a basis for hydrological modeling (Hollaus et al., 2005). LiDAR application delivers georeferenced surface elevation information from which digital elevation models (DEMs) can be produced. Surface elevation changes can be calculated from multi-temporal DEMs (Hopkinson et al., 2001; Kraus, 2004). In snow hydrology studies Terrestrial Laser Scanning (TLS) was applied to detect snow cover distribution, persistence of snow cover and accumulation gradients (Mott et al., 2010; Lehning et al., 2011; Schirmer et al., 2011) as well as the temporal evolution of snow ablation patterns (Egli et al., 2011; Mott et al., 2011). Only a restricted area can be investigated due to the fixed measurement site of the scanner.

Areas shaded by topography can not be recorded by the laser beam, which itself has a limited reach.

Application of LiDAR from aircraft, the so called Airborne Laser Scanning (ALS), enables covering whole catchments within one data acquisition. A data set of a series of ALS acquisitions was used in order to detect glacier volume changes in a subcatchment of the upper Rofen valley (46°48′ N, 10°46′ E) on annual and multi-annual time scales (Geist, 2005; Bollmann, 2010; Fischer, 2011). (Helfricht et al., 2012) derived SWE distribution and accumulation gradients of $8\,\%\,100\,\mathrm{m}^{-1}$ to $13\,\%\,100\,\mathrm{m}^{-1}$ in this high mountain catchment. Glacier volume changes were analyzed from a new glacier inventory for the Ötztal Alps based on ALS data (Abermann et al., 2009, 2010).

However, snow and ice-dynamical processes contribute to observed surface elevation changes on glacier surfaces. In this study surface elevation changes of the accumulation season ranging from the beginning of October (t_1) to the end of April and the beginning of May (t_2) are investigated. Figure 1 graphs the processes causing surface elevation changes on glaciers in this period. The elevation z_2 at the time t_2 corresponds to the primary surface z_1 at the time t_1. The accumulation of snow (ACC) at the time t_2 is defined as the elevation difference between the elevation of the actual surface z_3 and z_2 (Eq. 1). Processes of densification of snow and firn (DSF), ablation (ABL) and vertical ice flow (Δz_{ICE}) shift the primary surface z_1 in elevation and are summarized in Eq. (2). The surface elevation change measured by ALS (Δz_{ALS}) is the result of accumulation and the shifting of the primary surface (Eq. 3).

$$\mathrm{ACC} = z_3 - z_2 \tag{1}$$

$$\mathrm{DSF} + \mathrm{ABL} + \Delta z_{\mathrm{ICE}} = z_2 - z_1 \tag{2}$$

$$\Delta z_{\mathrm{ALS}} = \mathrm{ACC} + \mathrm{DSF} + \mathrm{ABL} + \Delta z_{\mathrm{ICE}} = z_3 - z_1 \tag{3}$$

The densification of snow and firn layers leads to an underestimation of the actual accumulation in the case of snow and firn layers on a static ice body. Ablation in terms of surface melt and basal melting contributes to this underestimation. Changes of the reference elevation due to vertical ice flow and ice thickness advection can have both,

Title Page

Abstract | Introduction

Conclusions | References

Tables | Figures

◄ | ►

◄ | ►

Back | Close

Full Screen / Esc

Printer-friendly Version

Interactive Discussion

negative and positive values. Submergent iceflow ($\Delta z_{ICE} < 0$) leads to an underestimation of ACC by Δz_{ALS}. Emergent ice flow ($\Delta z_{ICE} > 0$) causes overestimation of ACC by Δz_{ALS}.

"Ground truth" data are necessary to evaluate Δz_{ALS} for snow cover and mass bal-
5 ance studies (Huss et al., 2009; Koblet et al., 2010; Fischer, 2011).

We compared actual ACC in terms of calculated snow depths from Ground Penetrating Radar (GPR) measurements to Δz_{ALS} on glacier surfaces. A measurement set-up of snow depth probing, snow pits and GPR data was used to record snow depths along profiles on four glaciers located in the Ötztal Alps, to answer these questions:
10 (i) What is the magnitude and the sign of the deviations between ALS derived surface elevation changes and actually observed snow depths measured by GPR on the investigated glaciers?
(ii) Which are the processes that contribute to these deviations on glacier surfaces?
(iii) What implication do the deviations between ALS surface elevation changes and
15 actually observed snow depths have for the application of multi-temporal ALS for hydrological studies in the investigated catchments?

The calculated deviations between actual snow depths and Δz_{ALS} were intersected with optical extra-terrestrial remote sensing data of a LANDSAT scene to differentiate between accumulation areas and ablation areas of the glaciers.
20 After the introduction an overview of data and methods is given in Sect. 2. Conditions on the glaciers during ALS acquisitions are treated in more detail in Sect. 3. In Sect. 4 the results are presented and discussed. Finally conclusions are made about the applicability of surface elevation changes derived from ALS for snow cover studies in glacierized catchments.

2 Data and methods

2.1 Study sites

The study sites are located next to the alpine main ridge in the Ötztal Alps (46°48′ N, 10°46′ E, Fig. 2). This region is of interest to snow cover studies in view of an increasing use of melt water runoff for hydro power production, and of the prediction of flood events in the downstream valleys (Kirnbauer et al., 2009). Most of the associated catchments show a significant glaciation. Four of the largest glaciers in this mountain range, namely Hintereisferner, Kesselwandferner, Gepatschferner and Vernagtferner were chosen to evaluate Δz_{ALS} on glacier surface for snow cover studies. All of these glaciers are subject to scientific research for decades. Hintereisferner (HEF, 46°48′ N, 10°46′ E) has one of the world-wide longest mass balance series starting in 1953 (Hoinkes, 1970; Fischer, 2010; Fischer et al., 2012). Based on these data a variety of models with different complexity were evolved to compute glacier surface mass balance (Kuhn et al., 1999; Escher-Vetter et al., 2009). Ice thickness was measured by Span et al. (2005). Since 2001 a series of ALS acquisitions enabled the comparison of geodetic and direct glaciological measurements of mass balance on Hintereisferner (Bollmann, 2010; Fischer, 2011). Kesselwandferner (KWF, 46°50′ N, 10°48′ E) was subject to scientific studies investigating density profiles and deformation of firn layers (Ambach and Eisner, 1966). Mass balance data of Kesselwandferner are available back to the hydrological year 1952/1953 (Fischer et al., 2011a). A stakes network is being surveyed by geodetic measurements since 1964. Annual vertical and horizontal velocities were determined from this data (Span, 1999; Abermann et al., 2007). Gepatschferner (GF, 46°51′ N, 10°45′ E) is the largest glacier in this region. Ice thickness was measured by Massimo (1997). The evolution of volume and area since the Little Ice Age is summarized by Hartl (2010). Since 1964 the mass balance of Vernagtferner (VF, 46°52′ N, 10°49′ E) is measured with the direct glaciological method by the Commission for Glaciology, Bavarian Academy of Sciences and Humanities, Munich. In combination with a runoff gauge in front of the glacier tongue a series of

hydro-meteorological models was calibrated for energy balance and hydrological studies (Escher-Vetter et al., 2009). For this study glacier outlines of the four investigated glaciers derived from the Austrian glacier inventory of 2006 (Abermann et al., 2009) were updated based on ALS data of 2010 according to Abermann et al. (2010).

2.2 Ground penetrating radar

Ground Penetrating Radar (GPR) is an active sensing technique utilizing electromagnetic waves to locate targets or internal layers within materials (Daniels, 2005). The antenna transmits a regular sequence of pulses of electromagnetic energy into the ground, here the snow pack on the glacier. The transmitted signal is partly reflected at boundaries between two layers with different relative permittivity (ϵ'_r) within the analysed media. The receiver of the GPR system records the reflected signal. Measured travel times of the GPR signal can be converted into depths of the reflecting surface using assumptions about the signal wave speeds. In a snow pack ϵ'_r is a function of the mixing ratio between ice, air and liquid water (Lundberg et al., 2006). However, the proportion of liquid water, in terms of a wet snow pack, can alter ϵ'_r in a significant way (Frolov and Macheret, 1999; Sundström et al., 2012). The attenuation of the signal depends on the used frequency and ϵ'_r of the penetrated material. Higher signal frequencies deliver a higher vertical accuracy, but are more attenuated within materials with a high ϵ'_r. In cryospheric sciences GPR is used to detect permafrost within rocky ground (e.g. Hinkel et al., 2001), to measure ice thickness (e.g. Span et al., 2005; Fischer et al., 2007), ice- and firn layering (e.g. Spikes et al., 2004) as well as subglacial structures and liquid water content of snow and ice (e.g. Murray et al., 1997; Lundberg and Thunehed, 2000). Snow depth distribution and internal structures in the snow pack have been analysed by GPR techniques, too (Machguth et al., 2006; Heilig et al., 2009; Mitterer et al., 2011).

2.2.1 Field campaigns

Three GPR campaigns were conducted close to the time of ALS acquisition. Dates and snow sample information are displayed in Table 1.

At the end of accumulation season 2010/2011 GPR data were recorded at Vernagtferner by the Commission of Glaciology, Bavarian Academy of Sciences and Humanities (Munich, Germany). A RIS One GPR instrument from IDS (Pisa, Italy) with shielded 600 MHz antennas was used. The GPR was pulled by a snowmobile. At the first and the last point of the sections snow depths were measured by snow depth probing and coordinates were recorded with a hand-held GPS. Between these points the GPR data were received by driving the snowmobile with a uniform speed. In total more than 15 km of GPR profiles were conducted, divided into four longitudinal sections, three additional shorter sections in the accumulation zone and one cross section (Fig. 6). Snow densities were measured at six locations in the frame of the annually winter mass balance measurements at the glacier.

At the same date a GPR measurement campaign was conducted on Gepatschferner and Kesselwandferner. GPR data were recorded with a 3-D system from MALÅ (Malå, Sweden) with shielded 500 MHz antennas along a cross profile in the accumulation zone of Gepatschferner and a longitudinal profile at Kesselwandferner (Fig. 7). In total more than seven kilometers of profiles devided into 33 sections were investigated on ski. First and last points of the individual sections were georeferenced by DGPS. Additionally three snow pits were dug on Gepatschferner and one on the tongue of Kesselwandferner. While snow depth probings were performed along the GPR sections on Gepatschferner, snow depth probings and GPR data do not coincide on Kesselwandferner. Sample spacing is larger on Kesselwandferner than on Gepatschferner, caused by higher movement velocities by skiing downhill the glacier (Table 2).

At the end of the accumulation season 2011/2012 a GPR campaign was conducted to measure snow depth along longitudinal sections and cross sections on Hintereisferner and Kesselwandferner (Figs. 8 and 9). Skis were used to pull another IDS RIS

one system with shielded 400 MHz antennas. In total over 12 km of GPR data were recorded. Snow depth probings were conducted at every first and last point of the single sections and seven snow pits have been dug. All data points were georeferenced by DGPS.

5   Snow samples in terms of snow depth probing and snow pits were used to identify the depth of the seasonal snow layer according to the guidelines for measuring glacier mass balance (Kaser et al., 2003). These data provided the basis to calculate the signal propagation speed for GPR analysis. However, in the accumulation zone of a glacier it is difficult to define the previous falls surface by snow probing. This surface can be

10   either a firn cover or a layer formed by solid precipitation before the ALS flight. Therefore, GPR signal velocities were calculated from measured snow stratigraphies and snow densities derived from snow pits. Snow probe measurements are more reliable in the ablation area of glaciers for comparison with GPR results.

Snow GPR systems with signal frequencies of 400 MHz, 500 MHz and 600 MHz were used

15   within the three measurement campaigns. With an assumed maximum vertical resolution of up to one third of the wavelength, vertical resolution of the received signals is between 0.12 m (600 MHz) and 0.19 m (400 MHz). This is about the same magnitude as the accuracy of multi-temporal application of ALS. Horizontal resolution is related to the beam width as a function of the reflector depth and approximately 0.5 m. The

20   sample rate of GPR measurements was chosen in such a way, that distances between the data points are lower than the beam width of the signal. So quasi-continuous information could be tracked along the profiles based on known stratigraphies from snow depth probing and from snow pits. ALS point densities (Table 2) and points per meter of GPR data (Table 1) were comparable.

25   **2.2.2 Processing**

GPR raw data were processed applying the ReflexW software from Sandmeier Scientic Software (Karlsruhe, Germany). The single sections of the GPR profiles were georeferenced with coordinates recorded by GPS at the first and the last points of the

Title Page

Abstract | Introduction

Conclusions | References

Tables | Figures

◄ | ►

◄ | ►

Back | Close

Full Screen / Esc

Printer-friendly Version

Interactive Discussion

sections. Coordinates for each trace were calculated at equal distances. The surface signal reflection was set to time zero. Low frequency offsets and noise in the spectrum was filtered applying a dewow and bandpass filter. In a next step temporally time consistent signals were eliminated by background removal. To compensate for spherical divergence losses we applied gain functions. No migration was applied due to the spatial homogeneity and the low reflector depth relative to the high density of GPR measurements. The boundaries of the snow layers were picked and corrected to the zero phase change. The picks were exported with the attribute of the two-way-travel time. The single sections have been merged to continuous longitudinal and cross profiles.

Mean GPR signal velocities were calculated from the snow pit data. Snow depths from depth probing were used for validation of the derived signal velocities. Assuming that the snow surface and the ice surface are parallel, the slope of the surface has to be considered. The recorded GPR signal corresponds to the snow depth perpendicular to the surface, but snow depth from depth probing and snow pits are measured vertical. A correction due to the slope was applied to the measured snow depths (h_m) first (Eq. 4).

$$h_{cor} = h_m \cdot \cos(\alpha) \tag{4}$$

Signal velocities (v) for measurements on Gepatschferner and Kesselwandferner in 2011 and measurements on Hintereisferner and Kesselwandferner in 2012 were calculated following Eq. (5). The slope corrected snow depth (h_{cor}) and the two-way-travel times (twt) at the snow pit locations were used. A mean signal velocity ($\bar{v}$) was derived for each measurement campaign. The relative variation of the signal velocities (CV_r) is defined as the ratio of the range between maximum velocity and minimum

LiDAR snow cover studies on glacier surface

K. Helfricht et al.

Title Page

Abstract | Introduction

Conclusions | References

Tables | Figures

◄ | ►

◄ | ►

Back | Close

Full Screen / Esc

Printer-friendly Version

Interactive Discussion

velocity to the mean velocity (Eq. 6).

$$v = \frac{2 \cdot h_{cor}}{twt} \tag{5}$$

$$CV_r = 100 \cdot \left(\frac{v_{max} - v_{min}}{\bar{v}} \right) \tag{6}$$

According to Kovacs et al. (1995) ϵ'_r of the snow cover can be calculated from snow density (Eq. 7). Based on these values of ϵ'_r GPR signal velocities can be approximated (Eq. 8). This was done to compare signal velocities derived from GPR measurements and signal velocities calculated from measured snow densities. On Vernagtferner snow pits were not located on the GPR profiles. Therefore the Eqs. (7) and (8) were used to derive GPR signal velocities directly from measured snow densities.

$$\epsilon'_r = (1 + 0.851 \cdot \rho_s)^2 \tag{7}$$

$$v \approx \frac{0.3}{\sqrt{\epsilon'_r}} \tag{8}$$

Snow depth probings available directly at GPR profiles were compared to calculated snow depths from GPR measurements using the derived mean velocities. All exported twt have been transferred into snow depths (h_v) using the mean velocities for each measurement campaign (Eq. 9). To compare GPR snow depths with vertical measured ALS Δz, h_v were corrected by the slope leading to the final snow depth derived from GPR (h_{GPR}) following Eq. (10).

$$h_v = \frac{twt \cdot v}{2} \tag{9}$$

$$h_{GPR} = \frac{h_v}{\cos(\alpha)} \tag{10}$$

LiDAR snow cover studies on glacier surface

K. Helfricht et al.

Title Page

Abstract	Introduction
Conclusions	References
Tables	Figures

|◄ | ►|

◄ | ►

Back | Close

Full Screen / Esc

Printer-friendly Version

Interactive Discussion

Figure 5 shows the magnitude of corrections which have to be applied to vertical measured data as a function of snow depth and slope. In the same figure the frequency distribution of snow depths measured with GPR and the frequency distribution of the occurring slopes are shown. Most frequent snow depths were between 1.55 m and 1.65 m. The most frequent slopes were between 5° and 7°. Corrections, which therefore have to be applied, were mainly in the magnitude of 0.01 m to 0.1 m.

2.3 LiDAR data

LiDAR, also called laser scanning, is an active remote sensing technology (Baltsavias, 1999; Wehr and Lohr, 1999; Kraus, 2004). A laser signal is emitted and the travel time of the signal reflected at the surface is recorded. LiDAR measurements do not require any external light source. Terrestrial laser scanning (TLS) measurements are spatially limited due to the maximum signal distance and topographic shading. Airborne laser scanning (ALS) can be applied in remote mountain areas (Geist, 2005). The GPS referenced data provide 3-D information of the reflecting surface with a high point density and accuracy. Multiple reflections and full wave recordings deliver additional information about the reflecting surface. Based on these 3-D point data, the so-called point cloud, digital elevation models (DEMs) can be produced (Lui, 2008). Surface elevation changes can be detected from the difference of the DEMs of multi-temporal laser scan acquisitions. Accuracy of the position and the surface elevation information of each point is affected by the accuracy of the components of the aircraft, which measure location, roll and spin. These are the GPS system and the inertial measurement unit (IMU) (Joerg et al., 2012). Further the accuracy of the laser signal is affected by the beam width as a function of distance between the aircraft and the surface, and the inclination of the beam to the surface. Adjustments of the single stripes along the flight path can be done by comparing overlapping areas of the stripes. Accuracy of the resulting DEMs is a function of the point density and depends on the used interpolation algorithm. Bollmann et al. (2011) showed for DEMs derived from ALS data of the Hintereisferner region, that an accuracy better than ±0.15 m for slopes below 35° can be

Title Page

Abstract   Introduction

Conclusions   References

Tables   Figures

◄   ►

Back   Close

Full Screen / Esc

Printer-friendly Version

Interactive Discussion

estimated. Except very small areas, the glacier surface is inclined less than 20° at the investigated glaciers (Fig. 5).

In this study four laser scan acquisitions were used. They were conducted by Topscan using Optech devices mounted on Cesna aircrafts. Technical details can be seen in Table 2. Mean flight speed was between $65\,\mathrm{m\,s^{-1}}$ and $70\,\mathrm{m\,s^{-1}}$. Mean flight altitude ranged about 1000 m and 1200 m above ground. The laser had a frequency of 70 kHz. Scan frequencies of 36 Hz (Gemini device) and 40 Hz (ALTM 3100 device) were used. Maximum scan angles were between ±25° (Gemini device) and ±20° (ALTM 3100 device). Reference surfaces were measured within each campaign and the measured accuracy is listed in Table 2.

The last pulses of all ALS points within one pixel of the resulting the DEMs were averaged to a grid size of 1 m. Two DEMs are necessary to detect surface elevation changes (Δz_{ALS}) for snow cover studies in winter seasons: one of a ALS acquisition in fall (t_1) and one of a ALS aquisition in spring (t_2). These two DEMs have to be subtracted following Eq. (3), whereas $z_1 = z_{t_1}$ and $z_3 = z_{t_2}$.

Absolute deviations (Δh_{abs}) were calculated to analyse differences between ALS surface elevation change (Δz_{ALS}) and snow depth from GPR (h_{GPR}) (Eq. 11).

$$\Delta h_{\mathrm{abs}} = \Delta z_{\mathrm{ALS}} - h_{\mathrm{GPR}} \tag{11}$$

2.4 LANDSAT snow cover

For this study the process of firn densification was supposed to be one source for deviations of Δz_{ALS} from actually observed snow depths. Firn areas of glaciers can be delineated by application of spaceborne optical data (Nolin, 2011). LANDSAT data are available in a spatial resolution of 30 m to identify snow cover, firn cover and bare ice areas . The application of the LANDSAT scenes is limited by the discrepancy of the date of acquisition to the date of interest and the occurrence of clouds covering the surface information. A LANDSAT scene is available for the mountain region of Ötztal Alps at the 31 August 2009. The conditions of this scene fulfill all requirements in

terms of no clouds, no fresh fallen snow on the glaciers and an advanced state of snow ablation in late summer. Firn areas at glacier surface were delineated by applying the Normalized Difference Snow Index (NDSI, Hall et al., 1987). The delineated firn areas are a proxy for the minimum elevations of the equilibrium line altitude of the glaciers.

5 They are expected to have snow densification and ice dynamical processes causing submergence of the surface.

3 Additional measurements of local conditions

Surface elevation changes between the dates of field campaigns and ALS acquisitions have to be considered for analysis of the Δh_{abs}. As well information of the sur-

10 face at the date of the ALS acquisition in fall (t_1) necessary. Snow accumulation before the ALS flights in the higher elevated glacier areas in fall has to be considered when identifying the snow layers in the GPR analysis. Photographs and measurements of snow depths and snow densities taken in annual glacier mass balance field campaigns on the investigated glaciers were used for data analysis. Information on

15 the weather conditions before the ALS flights, between the ALS acquisitions and the field campaigns as well as on the weather conditions within the accumulation seasons were obtained from two automatic weather stations located next to Hintereisferner (46°47′55″ N,10°45′37″ E, 3027 m a.s.l.) and next to Vernagtferner (46°51′23″ N, 10°49′43″ E, 2640 m a.s.l., Fig. 2). The course of daily mean temperatures and cumu-

20 lative precipitation at the two automatic weather stations can be seen in Figs. 3 and 4. At 12 October 2010 snow depths and snow densities of a snow layer covering the 2010 firn layer on Gepatschferner and Kesselwandferner was measured by 43 snow depth probings and three snow pits. This snow layer was accumulated in September 2010. Within a warm period before the ALS flight this layer was transformed into

25 a highly dense snow pack with a crusted surface. The snow layer could be identified in the stratigraphies of spring firn pits and in the snow layering derived from GPR data in 2011. Snow depths of the snow layer accumulated in September 2010 were

measured within the annual mass balance measurements at Vernagtferner in fall by 34 snow probings. Between the ALS acquisition in spring 2011 and the corresponding GPR field campaigns a shallow snow cover of about 0.1 m with a low density was accumulated. In September 2011 a snowfall event formed a snow cover at the glaciers before ALS acquisition. This snow layer was exposed to clear sky and melt conditions for a longer time period. Photographs and snow samples from glacier mass balance measurements were used to estimate the depth of this layer at the time of ALS acquisition. Glacier tongues and steep south exposed glacier areas on Hintereisferner and Kesselwandferner appeared snow free on photographs taken within the annual mass balance measurements on 1 October 2011. Only a shallow snow layer was covering the firn areas (A. Fischer, personal communication, 2012). A few days after the ALS acquisition in October 2011 a snowfall event preserved the surface recorded by ALS from melt. The weather conditions enabled snow melt at the two days between the field campaigns and ALS acquisition in May 2012.

4   Results and discussion

Calculated velocities of the GPR signal for the single field campaigns are listed in Table 1. The mean signal velocity for GPR data on Vernagtferner was calibrated using the measured snow densities of 7 snow pits according to Kovacs et al. (1995), because snow pits were not located directly on the GPR profile. The CV_r of the calculated mean signal velocities is higher for 2012 data due to higher variations in measured densities at the snow pits.

The spatial distribution of Δz_{ALS} on the investigated glaciers and the calculated snow depths derived fom GPR measurements (h_{GPR}) along the profiles can be seen in Figs. 7 and 6. Locations of snow pits and snow depth probings of the spring field campaigns are included. Data of the individual profiles named in the figures are listed in Table 3. For further analysis the results for GPR points corresponding to LANDSAT pixels where firn was detected (labeled with "firn areas") and GPR points corresponding

1802

to LANDSAT pixels showing ice surface (labeled with "ice areas") were treated separately. Figure 10 shows the total number of analaysed data points on firn and on ice surfaces of the profiles and the statistical distribution of all absolute deviations Δh_{abs} (Eq. 11) in terms of the median (red line), the scatter (25 % and 75 % percentiles, blue box), the range of extreme values (black whiskers) and the outliers (red cross).

The medians of the box plots are a measure of whether the signs of the deviations are predominantly positive or negative. The interquartile range between the 25 % and 75 % percentiles shows the variabilty of the deviations due to surface roughness and random errors based on measurement methods and assumptions in data processing. Together, median and interquartile range highlight the significance of the deviations. The whiskers include all deviations within 1.5 times the interquartile range added to the 25 % percentile and to the 75 % percentile. Deviations due to locally enhanced snow and ice dynamical processes are contained within the range of the whiskers. Outliers are defined as deviations more than 1.5 times the interquartile range away from the 25 % percentile or from the 75 % percentile. Outliers can be related to presence of crevasse in ALS or GPR data.

The profile H1 is the complete longitudinal section on Hintereisferner. Figure 11 shows the distribution of Δz_{ALS} and h_{GPR} along the whole profile. Primarily negative deviations occur at data points of the firn area (Fig. 11, blue shaded areas). The crevassed areas in the upper part of the glacier cause a high variance in Δz_{ALS}. Only small deviations can be found along the glacier tongue below an elevation of 3100 m a.s.l. Values of Δz_{ALS} slightly exceed h_{GPR} at the glacier front.

The cross profile H2 is characterized by an alternation between convex crevassed areas with positive deviations and concave firn depression with negative deviations. Overall the median of negative deviations is higher than in the crevassed areas. The variation of the deviations is less in the ice areas of the profiles H3, H4 and H5 than in the higher elevated crevassed areas of Hintereisferner. A slight increase of the median of the deviations towards positive values can be seen from the uppermost cross profile

Title Page

Abstract | Introduction

Conclusions | References

Tables | Figures

|◄ | ►|

◄ | ►

Back | Close

Full Screen / Esc

Printer-friendly Version

Interactive Discussion

H3 towards the cross profile H5 on the glacier tongue. This is supposed to be an evidence for a slight increase of emergence flow towards the front of the glacier tongue.

The cross profile K1 is entirely located in the firn area of Kesselwandferner near to the snow line at the end of ablation season. Deviations are negative, but smaller than in the higher elevated glacier areas in profile K3. The profile K2 is located in a highly crevassed part of the glacier towards the ice divide between Gepatschferner and Kesselwandferner. One third of all measurement points of the profile have been delineated as located on bare ice. However, the deviations show nearly the same values, whether on firn or on ice. The profile K3 is situated in the accumulation area of Kesselwandferner. Here absolute deviations Δh_{abs} are increasingly negative in addition to an increase in measured snow depths. Thus, the increase of relative deviations Δh_{rel} is relatively small. The longitudinal profile K4 clearly shows the relation between firn areas and negative deviations (Fig. 12). While in the central part of the profile deviations are small, emergence is dominant on the front of the glacier tongue. At the cross profile K5 variation and median of the deviations are not indicating vertical ice flow (Figs. 9 and 10).

Detected firn areas from LANDSAT data are relatively small and probably do not cover the whole accumulation zone on Vernagtferner. This shifts the results of the deviations in the ice areas towards more negative values, as it is displayed by the whiskers of the profiles V1 and V5 in Fig. 10. However, even in the small firn areas the significant negative deviations are visible in the longitudinal profiles at Vernagtferner. Small deviations appear at the profile V6 in the upper part of Vernagtferner, both in firn and ice areas. The cross profile V7 shows a small variability in deviations and a median of the deviations next to zero. The data of the relatively short profile V8 confirm the negative deviations in firn areas.

The cross profile GP is restricted to the accumulation area of Gepatschferner. Ice areas could be differentiated from firn areas based on LANDSAT data even in the highest elevations of this large glacier plateau. Deviations at points identified as ice surface were less negative than those at points corresponding to firn areas. The profile K0

at Kesselwandferner ranges from the ice divide between Gepatschferner and Kessel-wandferner towards the glacier tongue of Kesselwandferner. This profile is showing positive deviations increasing towards the glacier tongue (Fig. 10).

Overall the distinction between firn covered areas and ice areas highlights the varying significance of the deviations of Δz_{ALS} from "ground truth" snow depth (here h_{GPR}) in different zones of the glaciers.

Submerging ice flow, firn densification and snow densification lead to a underestimation of snow depths by interpreting Δz_{ALS} as snow depth in present accumulation areas of the investigated glaciers. In these areas mean absolute deviation (Eq. 11) is −0.40 m with a mean standard deviation of 0.34 m. However, very locally relative deviations reach values of up to −40 % or more. In the bare ice areas mean absolute deviation is 0.004 m with a standard deviation of 0.27 m, in relative values −0.002 % with a standard deviation of 14.4 % respectively. An overestimation of snow depths by Δz_{ALS} was recognized at the very front of the glacier tongues.

Deviations at the delineated ice areas depend on the location of the profiles. Longitudinal profiles show a higher range of the deviations within the percentiles in comparison to cross profiles. This can be attributed to the shift of impact and sign of submergence and emergence processes along the flow line. Deviations at data points, which were delineated as ice but located near the firn line or surrounded by firn area, were close to the magnitude of deviations of firn points of the same profile, but mostly less negative.

Data were analysed in the original spatial resolution of 1 m and less. Both, in ALS and in GPR data, small scale heterogeneities of the surface are mapped. However, horizontal ice flow is shifting surface heterogeneities along the flow direction within one accumulation season. Hence, location of crevasses in fall are included in the data of Δz_{ALS}, whereas GPR data show the location of the crevasse in spring (e.g. Fig. 12 at a profile distance of 700 m). Comparing the sequence of maximum snow depths in both data sets, glacier flow velocities along the direction of the profile can be estimated. However, in the analysis of Δh_{abs} the horizontal shift is not considered. Resulting maximum deviations are displayed as outliers in the Fig. 10.

LiDAR snow cover studies on glacier surface

K. Helfricht et al.

The uncertainty of the results of this study depend on the accuracy of the used methods and the weather conditions close to the field campaigns. Like it is shown in Joerg et al. (2012), stochastic uncertainties of ALS derived surface elevations are strongly reduced on less inclined, homogeneous glacier surfaces. The mean standard deviation of deviations between ALS data and the elevations of a horizontal reference surface shown in Table 2 is about ±0.05 m. As mentioned in Sect. 2.3 a stochastic uncertainty for ALS surface elevation studies in mountain catchments of ±0.15 m is reasonable. Quality of the GPR data analysis depends strongly on the amount of additional information. While stochastic uncertainties are due to the vertical resolution of the used GPR frequency, systematic errors and stochastic uncertainties result from velocity assumptions and the non-automated analysis of the GPR data. To determine the actual GPR signal velocity, additional information exists only for singular points (e.g. snow pits, snow probing). These measurements contain errors and uncertainties themselves. For the analysis of GPR data between these points the characteristics of the snow cover influencing the GPR signal velocity like grain size, snow density, liquid water content or ice lenses are assumed to be constant. However, variability of snow depths calculated from GPR measurements along the profiles show a promising fit on the variability in snow depths derived from ALS. In the profile H1 on Hintereisferner (Fig. 11) for example, variations in Δz_{ALS} of more than 0.5 m are evident in h_{GPR} from the profile distance of 2000 m to the front of the glacier tongue.

An error analysis accounting for stochastic uncertainties in GPR velocity, vertical resolution of GPR data and uncertainties from ALS surface elevation changes results in a stochastic error of less than ±0.25 m for a mean snow depth of 1.5 m. This is slightly more than the interquartile range in the box plots (Fig. 10). The relative uncertainty of ±17 %, respectively, is in the same magnitude as the mean relative standard deviation of all profiles.

Mean systematic offset of each ALS acquisition was calculated based on a reference surface (Table 2). However, this systematic offset must not coincide with a systematic offset of the ALS data at the investigated glaciers. Due to the fact, that the systematic

Title Page

Abstract | Introduction

Conclusions | References

Tables | Figures

◄ | ►

◄ | ►

Back | Close

Full Screen / Esc

Printer-friendly Version

Interactive Discussion

offsets are smaller than the assumed vertical accuracy of ±0.15 m, no corrections have been applied to ALS data.

Systematic errors can be caused by errors in the calculation of the GPR signal velocities. The comparison of snow depths calculated from GPR data and slope corrected snow depths (h_{cor}) derived from 95 snow probings at Vernagtferner show a mean offset of −0.08 m with a standard deviation of 0.13 m, accounting for lower snow depths calculated from GPR data. This can be related to the usage of a snowmobile for GPR measurements. While GPR data were recorded in the track of the snowmobile, snow depth probings were performed beside the snowmobile in the undisturbed snow. A constant offset in the magnitude of less than 0.1 m seem to be reasonable and evident in the comparison. The comparison of GPR snow depths calculated with the mean signal velocity and snow depth probings show a mean deviation of 0.01 m with a standard deviation of 0.13 m at Hintereisferner and Kesselwandferner in 2012.

Overall in glacierized mountain catchments it is hard to coordinate the dates of maximum ablation in fall and maximum accumulation in spring with the ALS acquisitions. After the ALS acquisition in fall, progressing ablation can cause systematic errors in analysis of Δz at the glacier tongues. In spring, systematic errors will increase with an increasing temporal separation of ALS flights and GPR campaigns. However, both, the temporal offsets between GPR and ALS measurements and the dates of ALS acquisitions in relation to the weather conditions are in good accordance to the required accuracy based on the previous assumptions for this study (Sect. 3, Figs. 3 and 4).

Due to the small changes within the time between ALS acquisitions and GPR campaigns, simple assumptions were made for processes causing surface elevation changes. The thin layer of fresh snow in spring 2011 was neglected, because the snow was moved aside when pulling the GPR antenna over the snow surface on Gepatschferner and Kesselwandferner. On Vernagtferner this freshly fallen snow was assumed to be depleted by the used snowmobile. In 2012 the GPR campaign took place before the ALS acquisition. The snow depth reduction due to melt conditions is

LiDAR snow cover studies on glacier surface

K. Helfricht et al.

Title Page

Abstract | Introduction

Conclusions | References

Tables | Figures

|◄ | ►|

◄ | ►

Back | Close

Full Screen / Esc

Printer-friendly Version

Interactive Discussion

assumed to be in the magnitude of the immersion of the GPR antenna into the upper-most snow layer during the measurements.

To account for the densification of snow accumulated before the ALS acquisition in fall, measurements of the snow layer in 2010 can give a rough estimate. Mean mea-sured density of this snow layer was 380 kg m^{-3} in fall. Mean snow depth derived from 43 snow depth probings was 0.64 m with a standard deviation of 0.16 m. Measured snow depths range between 0.4 m and 1.05 m. Densities of the same snow layer mea-sured in spring 2011 were slightly increased with values of 410 kg m^{-3}. This difference would correspond to a compaction of 1 m snow depth by 0.07 m, 0.5 m snow depth by 0.04 m respectively. The mean snow depth of the snow probings on Vernagtferner in fall 2010 was 0.38 m with an standard deviation of 0.17 m. Measured snow depths were ranging from 0.2 m at the glacier tongue to a maximum of 0.93 m.

From this data comparison it is not feasible to asses the quantitative proportion of the particular processes contributing to deviations of Δz_{ALS} from actually observed snow depths. On Gepatschferner mean absolute deviation in ice areas of the profile G1 is −0.28 m, while firn points show a mean absolute deviation of −0.49 m. This gives a rough estimate for differences between deviations in areas attributed to ice flow and snow densification only and deviations in areas influenced by firn densification addi-tionally. For quantitive analysis of the single processes a more detailed and extensive measurement setup would be necessary.

The four investigated glaciers show different dynamical behavior influencing the in-terpretation of the ALS data in terms of snow cover for hydrological studies. Positive and negative deviations between Δz_{ALS} and h_{GPR} are evident at Kesselwandferner (Fig. 12). The derived deviations are in the magnitude of half the measured values of annual submergence and annual emergence shown in Abermann et al. (2007). Dis-tinct submergence processes were detected in the upper part of Gepatschferner. In the uppermost parts of Hintereisferner negative deviations occur between the crevassed areas (Fig. 11). No clear evidence of deviations induced by vertical ice flow is visible at the larger part of the glacier tongue of Hintereisferner. Submergence flow could be

Title Page

Abstract | Introduction

Conclusions | References

Tables | Figures

|◄ | ►|

◄ | ►

Back | Close

Full Screen / Esc

Printer-friendly Version

Interactive Discussion

detected only at the very front of the glacier tongue of Hintereisferner. These results coincide with the findings of Fischer et al. (2011b). They showed that the majority of annual deviations between direct and geodetic glacier mass balance measurements are located in the accumulation zone of Hintereisferner. Deviations between Δz_{ALS} and h_{GPR} are close to zero in most parts of Vernagtferner. This can be related to the recently reduced dynamics of the glacier (Khazaleh, 2002).

At the majority of the area of the four investigated glaciers relative deviations of the ALS measurements from actually observed snow depths are less than assumed errors of measurement of solid precipitation in high mountain catchments. The information on snow accumulation from Δz_{ALS} in these catchments is supposed to be a more reliable measurement not only of the spatial distribution of snow accumulation, but also for total catchment precipitation. The maps of spatial distribution of Δz_{ALS} can be transferred into SWE using simple regression methods (Jonas et al., 2009; Schöber et al., 2012a). Again these maps can be used for calibration and validation of hydro-meteorological models in the investigated catchment.

5 Conclusions

The study presented here was accomplished to evaluate surface elevation changes derived from ALS (Δz_{ALS}) on glacier surfaces for snow cover studies in a glacierized catchment of the Ötztal Alps. Therefore, deviations of Δz_{ALS} from actually observed snow depths of more than 35 km of GPR profiles on four glaciers were analysed. The magnitude of the sum of all processes contributing to the observations could be detected by the method combination of ALS and GPR data. It is shown that the delineating of glacier firn areas from LANDSAT data is an useful tool to get an overview of areas where deviations of Δz_{ALS} are significantly negative. This underestimation is mainly caused by the processes of submergence ice flow, firn densification and densification of snow accumulated before the ALS acquisition in fall. Areas delineated as bare ice show on average no significant deviations on the investigated glaciers. Emergence ice

flow could be detected only at the very front of the glacier tongues. Overall the mean measured deviations of Δz_{ALS} are small in comparison to assumed errors of precipitation measurements in high mountain catchments. Hence, maps of SWE calculated from Δz_{ALS} at glacier surface are a spatial information of a minimum water storage
5 which should be simulated by hydro-meteorological models, particularly in the higher elevated parts of the glaciers in this region. The knowledge gained about deviations of Δz_{ALS} from actually observed snow depths on these glaciers can be integrated in the calibration and validation process of hydro-meteorological models for a more realistic simulation of the heterogeneity of the mountain snow cover.

References

20 Abermann, J., Schneider, H., and Lambrecht, A.: Analysis of surface elevation changes on Kesselwand glacier – comparison of different methods, Zeitschrift für Gletscherkunde und Glazialgeologie, 41, 147–167, 2007. 1793, 1808
Abermann, J., Lambrecht, A., Fischer, A., and Kuhn, M.: Quantifying changes and trends in glacier area and volume in the Austrian Ötztal Alps (1969-1997-2006), The Cryosphere, 3,
25 205–215, doi:10.5194/tc-3-205-2009, 2009. 1791, 1794
Abermann, J., Fischer, A., Lambrecht, A., and Geist, T.: On the potential of very high-resolution repeat DEMs in glacial and periglacial environments, The Cryosphere, 4, 53–65, doi:10.5194/tc-4-53-2010, 2010. 1791, 1794

Ambach, W. and Eisner, H.: Analysis of a 20 m firn pit on the Kesselwandferner (Ötztal Alps)., J. Glaciol., 6, 223–231, 1966. 1793

Aschwanden, H., Weingartner, R., and Leibundgut, C.: Zur regionalen Übertragung von Mittelwertendes Abflusses – Teil 1: Raumtypisierung der Abflussregime der Schweiz., Deutsche Gewässerkundliche Mittleilungen, 30, 52–61, 1986.

Baltsavias, E.: Airborne laser scanning: basic relations and formulas, ISPRS Journal of Photogrammetry and Remote Sensing, 54, 199–214, doi:10.1016/S0924-2716(99)00015-5, 1999. 1789

Baños, I. M., Garcia, A. R., i Alevadra, J. M., i Figueras, P. O., Iglesias, J. P., i Figueras, P. M., and López, J. T.: Assessment of airborne LIDAR for snowpack depth modeling, Boletin de la Sociedad Geológica Mexicana, 63, 95–2011, 2011. 1799
1789

Bernhardt, M., Liston, G. E., Strasser, U., Zängl, G., and Schulz, K.: High resolution modelling of snow transport in complex terrain using downscaled MM5 wind fields, The Cryosphere, 4, 99–113, doi:10.5194/tc-4-99-2010, 2010. 1789

Bollmann, E.: Airborne Laser Scanning Glacier Mass Balance, Master's thesis, University of Innsbruck, Institute for Geography, 2010. 1791, 1793

Bollmann, E., Sailer, R., Briese, C., Stötter, J., and Fritzmann, P.: Potential of airborne laser scanning for geomorphologic feature and process detection and quantifications in high alpine mountains, Z. Geomorphol. Supp., 55, 83–104, doi:10.1127/0372-8854/2011/0055S2-0047, 2011. 1799

Dadic, R., Mott, R., Lehning, M., and Burlando, P.: Wind influence on snow depth distribution and accumulation over glaciers, J. Geophys. Res., 115, F01012, doi:10.1029/2009JF001261, 2010. 1789

Daniels, D. J.: Ground Penetrating Radar, John Wiley & Sons, Inc., doi:10.1002/0471654507.eme152, 2005. 1794

Egli, L., Jonas, T., Grünewald, T., Schirmer, M., and Burlando, P.: Dynamics of snow ablation in a small Alpine catchment observed by repeated terrestrial laser scans, Hydrol. Process., 26, 1574–1585, doi:10.1002/hyp.8244, 2012. 1790

Escher-Vetter, H., Kuhn, M., and Weber, M.: Four decades of winter mass balance of Vernagtferner and Hintereisferner, Austria: methodology and results, Ann. Glaciol., 50, 87–95, doi:10.3189/172756409787769672, 2009. 1790, 1793, 1794

LiDAR snow cover studies on glacier surface

K. Helfricht et al.

Title Page

Abstract | Introduction

Conclusions | References

Tables | Figures

◄◄ | ►►

◄ | ►

Back | Close

Full Screen / Esc

Printer-friendly Version

Interactive Discussion

Fierz, C., Armstrong, R., Durand, Y., Etchevers, P., Greene, E., McClung, D., Nishimura, K., Satyawali, P., and Sokratov, S.: The International Classification for Seasonal Snow on the Ground, Tech. rep., IHP-VII Technical Documents in Hydrology No. 83, IACS Contribution No. 1, UNESCO-IHP, Paris, 2009. 1790

5 Fischer, A.: Glaciers and climate change: interpretation of 50 years of direct mass balance of Hintereisferner, Global Planet. Change, 71, 13–26, doi:10.1016/j.gloplacha.2009.11.014, 2010. 1790, 1793

Fischer, A.: Comparison of direct and geodetic mass balances on a multi-annual time scale, The Cryosphere, 5, 107–124, doi:10.5194/tc-5-107-2011, 2011. 1791, 1792, 1793

10 Fischer, A., Span, N., Fischer, A., Kuhn, M., Massimo, M., and Butschek, M.: Radarmessungen der Eisdicke Österreichischer Gletscher. Band II: Messungen 1999 bis 2006, Österreichische Beiträge zu Meteorologie und Geophysik, 33, 142 pp., 2007. 1794

Fischer, A., Markl, G., Kuhn, M., Schneider, H., and Abermann, J.: Glacier Mass Balance of Kesselwandferner, Oetztal Alps, Austria, from 1952/53-2009/11., World Data Center for Climate, doi:10.1594/WDCC/MB_KWF_1953-2011, 2011a. 1793

15 Fischer, A., Schneider, H., Merkel, G., and Sailer, R.: Comparison of direct and geodetic mass balances on an annual time scale, The Cryosphere Discuss., 5, 565–604, doi:10.5194/tcd-5-565-2011, 2011b. 1809

Fischer, A., Markl, G., and Kuhn, M.: Glacier Mass Balance of Hintereisferner, Ötztal Alps, Austria, from 1952/53–2010/11, doi:10.1594/WDCC/MB_HEF_1953-2011, 2012. 1793

20 Frolov, A. D. and Macheret, Y. Y.: On dielectric properties of dry and wet snow, Hydrol. Process., 13, 1755–1760, doi:10.1002/(SICI)1099-1085(199909)13:12/13<1755::AID-HYP854>3.0.CO;2-T, 1999. 1794

Geist, T.: Application of airborne laser scanning technology in glacier research, Ph.D. thesis, Institute of Geography, University of Innsbruck, Austria, 2005. 1791, 1799

25 Hall, D. K., Ormsby, J. P., Bindschadler, R. A., and Siddalingaiah, H.: Characterization of snow and ice reflectance zones on glaciers using Landsat thematic mapper data, Ann. Glaciol., 9, 104–108, 1987. 1801

Hall, D. K., Riggs, G. A., Salomonson, V. V., DiGirolamo, N. E., and Bayr, K. J.: MODIS snow-cover products, Remote Sens. Environ., 83, 181–194, doi:10.1016/S0034-4257(02)00095-0, 2002. 1790

LiDAR snow cover studies on glacier surface

K. Helfricht et al.

Title Page

| Abstract | Introduction |

| Conclusions | References |

| Tables | Figures |

|◄ | ►|

| ◄ | ► |

| Back | Close |

Full Screen / Esc

Printer-friendly Version

Interactive Discussion

Hartl, L.: The Gepatschferner from 1850–2006. Changes in Length, Area and Volume in Relation to Climate, Master's thesis, Institute for Meteorology and Geophysics, University of Innsbruck, 2010. 1793

Heilig, A., Schneebeli, M., and Eisen, O.: Upward-looking ground-penetrating radar for monitoring snowpack stratigraphy, Cold Reg. Sci. Technol., 59, 152–162, doi:10.1016/j.coldregions.2009.07.008, 2009. 1794

Helfricht, K., Schöber, J., Seiser, B., Fischer, A., Stötter, J., and Kuhn, M.: Snow accumulation of a high alpine catchment derived from LiDAR measurements, Adv. Geosci., 32, 31–39, doi:10.5194/adgeo-32-31-2012, 2012. 1791

Hinkel, K. M., Doolittle, J. A., Bockheim, J. G., Nelson, F. E., Paetzold, R., Kimble, J. M., and Travis, R.: Detection of subsurface permafrost features with ground-penetrating radar, Barrow, Alaska, Permafrost Periglac., 12, 179–190, doi:10.1002/ppp.369, 2001. 1794

Hoinkes, H.: Methoden und Möglichkeiten von Massenhaushaltsstudien auf Gletschern, Zeitschrift für Gletscherkunde und Glazialgeologie, 6, 37–90, 1970. 1793

Hollaus, M., Wagner, W., and Kraus, K.: Airborne laser scanning and usefulness for hydrological models, Adv. Geosci., 5, 57–63, doi:10.5194/adgeo-5-57-2005, 2005. 1790

Hopkinson, C., Sitar, M., Chasmer, L., Gynan, C., Agro, D., Enter, R., Foster, J., Heels, N., Hoffman, C., Nillson, J., and St. Pierre, R.: Mapping the Spatial Distribution of Snowpack Depth Beneath a Variable Forest Canopy Using Airborne Laser Altimetry, Proccedings of the 58th Annual Eastern Snow Conference, Ottawa, Canada, 2001. 1790

Huss, M., Farinotti, D., Bauder, A., and Funk, M.: Modelling runoff from highly glacierized alpine drainage basins in a changing climate, Hydrol. Process., 22, 3888–3902, doi:10.1002/hyp.7055, 2008. 1789

Huss, M., Bauder, A., and Funk, M.: Homogenization of long-term mass-balance time series, Ann. Glaciol., 50, 198–206, doi:10.3189/172756409787769627, 2009. 1792

Joerg, P. C., Morsdorf, F., and Zemp, M.: Uncertainty assessment of multi-temporal airborne laser scanning data: a case study on an Alpine glacier, Remote Sens. Environ., 127, 118–129, doi:10.1016/j.rse.2012.08.012, 2012. 1799, 1806

Jonas, T., Marty, C., and Magnusson, J.: Estimating the snow water equivalent from snow depth measurements in the Swiss Alps, J. Hydrol., 378, 161–167, doi:10.1016/j.jhydrol.2009.09.021, 2009. 1809

Title Page

Abstract | Introduction

Conclusions | References

Tables | Figures

◀ | ▶

◀ | ▶

Back | Close

Full Screen / Esc

Printer-friendly Version

Interactive Discussion

Kaser, G., Fountain, A., and Jansson, P.: A manual for monitoring the mass balance of mountain glaciers, International Hydrological Programme, IHP-VI. Technical Documents in Hydrology 59, UNESCO, Paris, 2003. 1796

Khazaleh, T.: Die oberflächliche, horizontale Eisgeschwindigkeit des Vernagtferner im Zeitraum 1986–2001, Master's thesis, Lehrstuhl der Physischen Geographie der Universität Augsburg, Kommission für Glaziologie der Bayerischen Akademie der Wissenschaften, München, 2002. 1809

Kirnbauer, R., Achleitner, S., Schöber, J., Asztalos, J., and Schönlaub, H.: Hochwasservorhersage Inn: Modellierung der Gletscherabflüsse, Mitteilungsblatt des Hydrographischen Dienstes in Österreich, Nr. 86, 109–130, 2009. 1793

Koblet, T., Gärtner-Roer, I., Zemp, M., Jansson, P., Thee, P., Haeberli, W., and Holmlund, P.: Reanalysis of multi-temporal aerial images of Storglaciären, Sweden (1959–99) – Part 1: Determination of length, area, and volume changes, The Cryosphere, 4, 333–343, doi:10.5194/tc-4-333-2010, 2010. 1792

Kovacs, A., Gow, A. J., and Morey, R. M.: The in-situ dielectric constant of polar firn revisited, Cold Reg. Sci. Technol., 23, 245–256, doi:10.1016/0165-232X(94)00016-Q, 1995. 1798, 1802

Kraus, K.: Geometrische Informationen aus Photographien und Laserscanaufnahmen, Band 1, Walter de Gruyter, Berlin, New York, 2004. 1790, 1799

Kuhn, M.: Verification of a hydrometeorological model of glacierized basins, Ann. Glaciol., 31, 15–18, doi:10.3189/172756400781820228, 2000. 1789

Kuhn, M.: Redistribution of snow and glacier mass balance from a hydrometeorological model, J. Hydrol., 282, 95–103, doi:10.1016/S0022-1694(03)00256-7, 2003. 1789

Kuhn, M. and Batlogg, N.: Glacier runoff in Alpine headwaters in a changing climate, Hydrology, Water Resources and Ecology in Headwaters, in: Proceedings of the HeadWater'98 Conference held at Meran/Merano, Italy, April 1998, IAHS Publication, 248, 79–88, 1998. 1789

Kuhn, M., Dreiseitl, E., Hofinger, S., Markl, G., Span, N., and Kaser, G.: Measurements and models of the mass balance of Hintereisferner, Geogr. Ann. A, 81, 659–670, doi:10.1111/1468-0459.00094, 1999. 1793

Lehning, M., Völksch, I., Gustafsson, D., Nguyen, T. A., Stähli, M., and Zappa, M.: ALPINE3D: a detailed model of mountain surface processes and its application to snow hydrology, Hydrol. Process., 20, 2111–2128, doi:10.1002/hyp.6204, 2006. 1789

LiDAR snow cover studies on glacier surface

K. Helfricht et al.

Title Page

Abstract | Introduction

Conclusions | References

Tables | Figures

|◀ | ▶|

◀ | ▶

Back | Close

Full Screen / Esc

Printer-friendly Version

Interactive Discussion

Lehning, M., Grünewald, T., and Schirmer, M.: Mountain snow distribution governed by an altitudinal gradient and terrain roughness, Geophys. Res. Lett., 38, L19504, doi:10.1029/2011GL048927, 2011. 1790

Lui, X.: Airborne LiDAR for DEM generation: some critical issues, Prog. Phys. Geog., 32, 31–49, doi:10.1177/0309133308089496, 2008. 1799

Lundberg, A. and Thunehed, H.: Impulse raaar snow surveys – influence of snow density, Nord. Hydrol., 3, 1–14, 2000. 1794

Lundberg, A., Richardson-Näslund, C., and Andersson, C.: Snow density variations: consequences for ground-penetrating radar, Hydrol. Process., 20, 1483–1495, doi:10.1002/hyp.5944, 2006. 1794

Lundberg, A., Granlund, N., and Gustafsson, D.: Towards automated "Ground truth" snow measurements a review of operational and new measurement methods for Sweden, Norway, and Finland, Hydrol. Process., 24, 1955–1970, doi:10.1002/hyp.7658, 2010. 1790

Machguth, H., Eisen, O., Paul, F., and Hoelzle, M.: Strong spatial variability of accumulation observed with helicopter-borne GPR on two adjacent Alpine glaciers, Geophys. Res. Lett., 33, L13503, doi:10.1029/2006GL026576, 2006. 1794

Massimo, M.: Eisdicke des Gepatschferners – Messungen mit dem Radio-Echolot, Master's thesis, Institute for Meteorology and Geophysics, University of Innsbruck, 1997. 1793

Mitterer, C., Heilig, A., Schweizer, J., and Eisen, O.: Upward-looking ground-penetrating radar for measuring wet-snow properties, Cold Reg. Sci. Technol., 69, 129–138, doi:10.1016/j.coldregions.2011.06.003, 2011. 1794

Mott, R., Schirmer, M., Bavay, M., Grünewald, T., and Lehning, M.: Understanding snow-transport processes shaping the mountain snow-cover, The Cryosphere, 4, 545–559, doi:10.5194/tc-4-545-2010, 2010. 1789, 1790

Mott, R., Egli, L., Grünewald, T., Dawes, N., Manes, C., Bavay, M., and Lehning, M.: Micrometeorological processes driving snow ablation in an Alpine catchment, The Cryosphere, 5, 1083–1098, doi:10.5194/tc-5-1083-2011, 2011. 1790

Murray, T., Gooch, D., and Stuart, G.: Structures within the surge front at Bakaninbreen, Svalbard, using ground-penetrating radar, Ann. Glaciol., 24, 122–129, 1997. 1794

Nolin, A. W.: Recent advances in remote sensing of seasonal snow, J. Glaciol., 56, 1141–1150, doi:10.3189/002214311796406077, 2011. 1790, 1800

Title Page

Abstract | Introduction

Conclusions | References

Tables | Figures

◀ | ▶

◀ | ▶

Back | Close

Full Screen / Esc

Printer-friendly Version

Interactive Discussion

Schirmer, M., Wirz, V., Clifton, A., and Lehning, M.: Persistence in intra-annual snow depth distribution: 1. Measurements and topographic control, Water Resour. Res., 47, W09516, doi:10.1029/2010WR009426, 2011. 1789, 1790

Schöber, J., Achleitner, S., Kirnbauer, R., Schöberl, F., and Schönlaub, H.: Hydrological modelling of glacierized catchments focussing on the validation of simulated snow patterns – applications within the flood forecasting system of the Tyrolean river Inn, Adv. Geosci., 27, 99–109, doi:10.5194/adgeo-27-99-2010, 2010. 1790

Schöber, J., Achleithner, S., Bellinger, J., Schneider, K., Kirnbauer, R., and Schöberl, F.: Spatial and temporal characteristics of the alpine snow cover: 1. Empirical basis for regional and watershed scale applications, J. Hydrol., submitted, 2012a. 1809

Schöber, J., Achleitner, S., Kirnbauer, R., Schöberl, F., and Schönlaub, H.: Impact of snow state variation for design flood simulations in glacierized catchments, Adv. Geosci., 31, 39–48, doi:10.5194/adgeo-31-39-2012, 2012b. 1789

Sevruk, B.: Correction of precipitation measurements: swiss experience, WMO/TD, 104, 187–196, 1985. 1790

Span, N.: Zur Dynamik des Kesselwandferners, Ph.D. thesis, Institute of Meteorology and Geophysics, University of Innsbruck, 1999. 1793

Span, N., Fischer, A., Kuhn, M., Massimo, M., and Butschek, M.: Radarmessungen der Eisdicke Österreichischer Gletscher. Band I: Messungen 1995 bis 1998., Österreichische Beiträge zu Meteorologie und Geophysik, 33, 145 pp., 2005. 1793, 1794

Spikes, V. B., Hamilton, G. S., Arcone, S. A., Kaspari, S., and Mayewski, P. A.: Variability in accumulation rates from GPR profiling on the West Antarctic plateau, Ann. Glaciol., 39, 238–244, doi:10.3189/172756404781814393, 2004. 1794

Strasser, U.: Modelling of the mountain snow cover in the Berchtesgaden National Park, Berchtegaden National Park research report, Nr. 55, 2008. 1789

Sundström, N., Kruglyak, A., and Friborg, J.: Modeling and simulation of GPR wave propagation through wet snowpacks: testing the sensitivity of a method for snow water equivalent estimation, Cold Reg. Sci. Technol., 74–75, 11–20, doi:10.1016/j.coldregions.2012.01.006, 2012. 1794

Wehr, A. and Lohr, U.: Airborne laser scanning – an introduction and overview, ISPRS Journal of Photogrammetry and Remote Sensing, 54, 68–82, doi:10.1016/S0924-2716(99)00011-8, 1999. 1799

LiDAR snow cover studies on glacier surface

K. Helfricht et al.

Title Page

Abstract	Introduction
Conclusions	References
Tables	Figures

|◀ | ▶|

◀ | ▶

Back | Close

Full Screen / Esc

Printer-friendly Version

Interactive Discussion

Zemp, M., Hoelzle, M., and Haeberli, W.: Six decades of glacier mass-balance observations: a review of the worldwide monitoring network, Ann. Glaciol., 50, 101–111, doi:10.3189/172756409787769591, 2009. 1790

Title Page

Abstract | Introduction

Conclusions | References

Tables | Figures

|◀ | ▶|

◀ | ▶

Back | Close

Full Screen / Esc

Printer-friendly Version
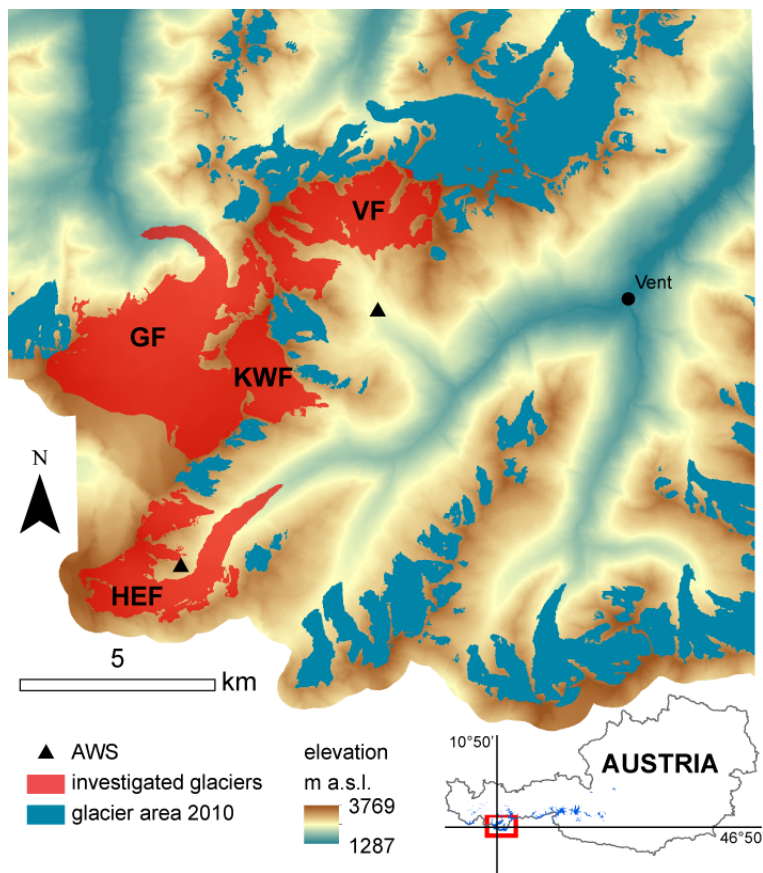
Interactive Discussion

Title Page

Abstract | Introduction

Conclusions | References

Tables | Figures

◄ | ►

Back | Close

Full Screen / Esc

Table 1. Attributes of the field measurements in spring. Number of snow depth probings and snow pits shown in brackets indicate measurements not directly located at the GPR profiles. The GPR signal velocities derived from snow stratigraphies in the snow pits (v_p) and GPR signal velocities calculated from measured snow densities (v_k) using Eqs. (7) and (8) with the corresponding coefficient of variation (CV, Eq. 6).

ID	date	GPR profile length (10^3 m)	mean GPR spacing (m)	snow depth probings	snow pits	signal velocity (m ns^{-1})			
						v_p	CV$_p$(%)	v_k	CV$_k$ (%)
VF	28–29 Apr 2011	15.32	0.35	102	1(6)	–	–	0.2254	3.9
GF	28 Apr 2011	5.39	0.30	33	3(1)	0.2270	2.0	0.2263	1.3
KWF	28 Apr 2011	1.84	0.45	0(17)	2				
HEF	9 May 2012	7.66	0.25	49	5	0.2254	9.6	0.2254	7.7
KWF	8 May 2012	5.19	0.18	31	2				

LiDAR snow cover
studies on glacier
surface

K. Helfricht et al.

Table 2. Overview of the ALS flight campaigns investigated in this study. The verticalaccuracy is obtained from deviations between ALS surface elevations and elevations of a known reference surface. The vertical accuracy is shown in terms of a mean deviation (mean) and the standard deviation (σ).

Timestamp	date	laser system	mean point density per m^2	vertical accuracy (m) mean	σ
t_1	7–10 Oct 2010	ALTM Gemini	3.6	0.071	0.047
t_2	20–23 Apr 2011	ALTM Gemini	3.8	−0.007	0.041
t_1	4 Oct 2011	ALTM 3100	2.9	0.001	0.042
t_2	11 May 2012	ALTM 3100	2.8	0.005	0.057

Table 3. Properties of the GPR profiles in terms of ID, profile length, minimum elevation and maximum elevation. Mean value of the surface elevation changes derived from ALS data $\overline{\Delta z}_{ALS}$ (Eq. 1) and the mean absolute deviation of this value from mean GPR snow depth $\overline{\Delta h}_{abs}$ (Eq. 11) are shown for firn areas and ice areas of each profile.

Profile ID	length (m)	elevation (m a.s.l.) max	elevation (m a.s.l.) min	ice areas (m) $\overline{\Delta z}_{ALS}$	ice areas (m) $\overline{\Delta h}_{abs}$	firn areas (m) $\overline{\Delta z}_{ALS}$	firn areas (m) $\overline{\Delta h}_{abs}$
H1	5788	3364	2532	2.32	−0.01	3.10	−0.50
H2	586	3159	3096	3.00	0.31	2.95	−0.38
H3	414	2905	2895	2.73	0.02	2.46	−0.47
H4	498	2754	2736	2.27	0.10	–	–
H5	176	2565	2557	1.33	0.07	–	–
K1	550	3175	3164	–	− 2.26	−0.32	
K2	6576	3210	3174	1.72	−0.19	1.94	−0.15
K3	1207	3293	3210	–	–	2.23	−0.60
K4	2485	3293	3019	2.43	0.23	2.32	−0.26
K5	291	3087	3072	2.33	0.02	–	–
G1	5391	3484	3154	1.38	−0.28	1.23	−0.49
K0	1844	3212	3035	1.76	0.29	1.52	0.04
V1	3458	3370	2803	1.61	−0.01	1.25	−0.35
V2	2022	3303	2892	1.54	0.00	1.79	−0.23
V3	2093	3307	2961	1.56	0.02	1.55	−0.10
V4	2412	3327	2864	1.47	0.01	1.48	−0.22
V5	1488	3355	3091	1.67	−0.08	1.36	−0.28
V6	1007	3264	3131	1.54	−0.05	1.66	−0.03
V7	2526	3060	3020	1.62	0.01	1.50	−0.05
V8	314	3303	3255	–	–	1.57	−0.22
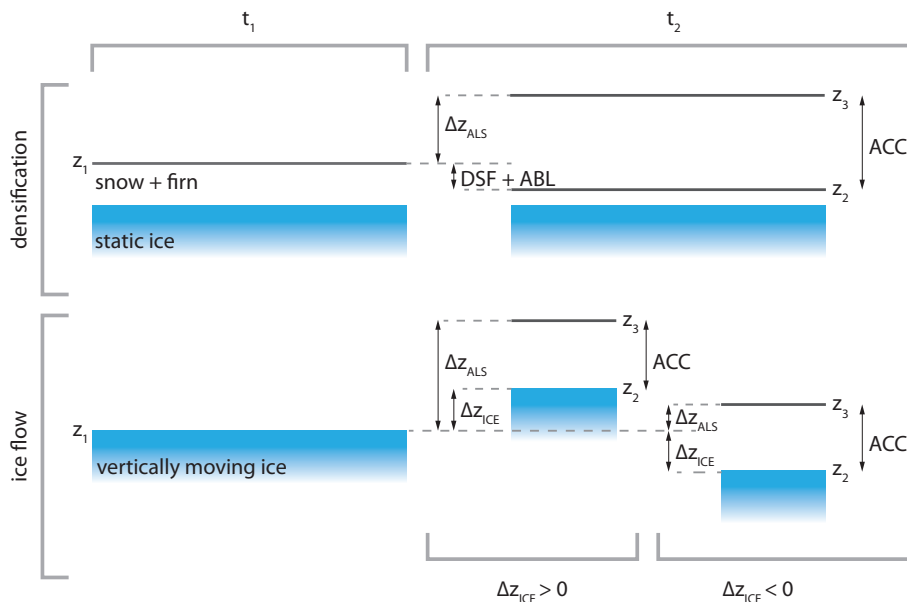
Fig. 1. Chart of the processes causing deviations between ALS surface elevation changes Δz_{ALS} and actual accumulation (ACC), namely densification of snow and firn (DSF), ablation (ABL) and vertical ice flow (Δz_{ICE}).

Fig. 2. Map of the investigation area next to Vent in the Ötztal Alps showing the locations of the glaciers Hintereisferner (HEF), Gepatschferner (GF), Kesselwandferner (KWF) and Vernagt-ferner (VF) and the automatic weather-stations (triangles).
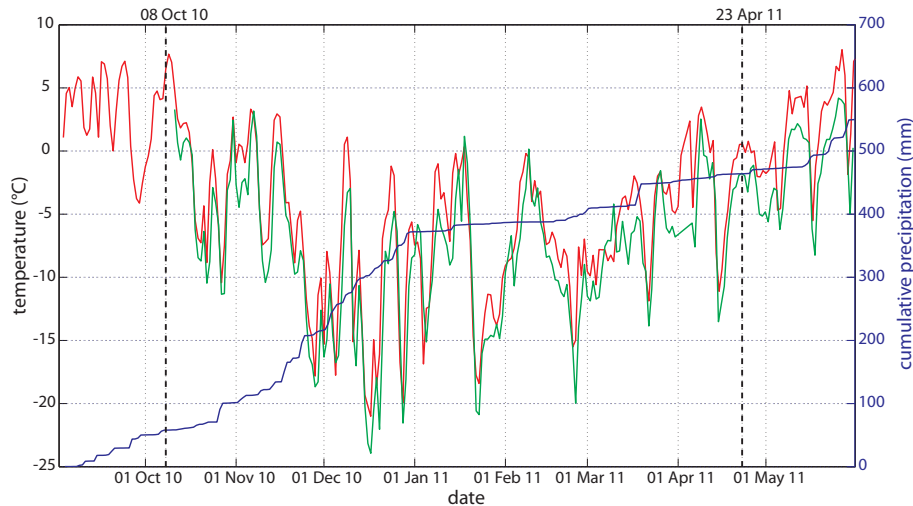
Fig. 3. Mean daily air temperature measured at the automatic weather station (AWS, Fig. 2) Hintereisferner (3027 m a.s.l., green curve) and the AWS Vernagtferner (2640 m a.s.l., red curve) for the accumulation season 2010/2011. Cumulative precipitation is shown for the AWS Vernagtferner (blue curve). Dates of ALS acquisitions are marked as dotted lines.

LiDAR snow cover studies on glacier surface

K. Helfricht et al.

Printer-friendly Version

Interactive Discussion

Fig. 4. Mean daily air temperature measured at the automatic weather station (AWS, Fig. 2) Hintereisferner (3027 m a.s.l., green curve) and the AWS Vernagtferner (2640 m a.s.l., red curve) for the accumulation season 2011/2012. Cumulativ precipitation is shown for the AWS Venagtferner (blue curve). Dates of ALS acquisitions are marked as dotted lines.
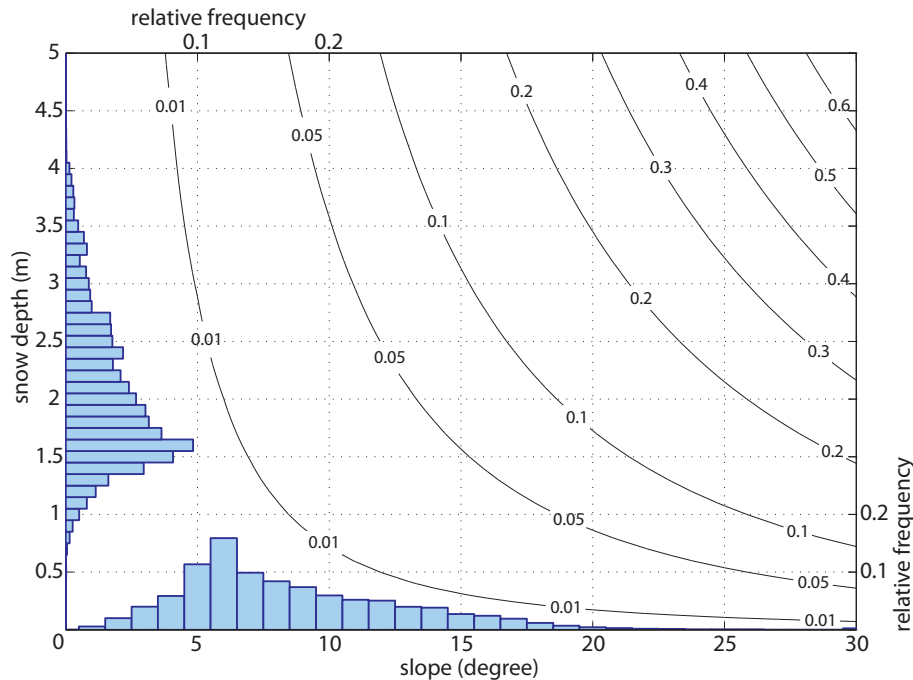
Fig. 5. Contour lines of the correction of GPR snow depth as a function of slope and snow depth. The relative frequency distribution of GPR snow depths h_v and the frequency distribution of the occuring slopes are presented in horizontal and vertical bars, respectively.
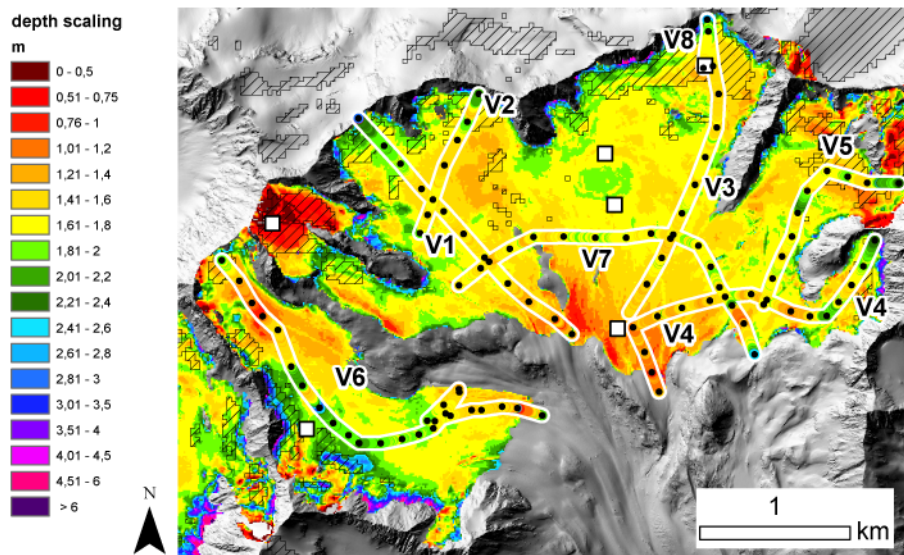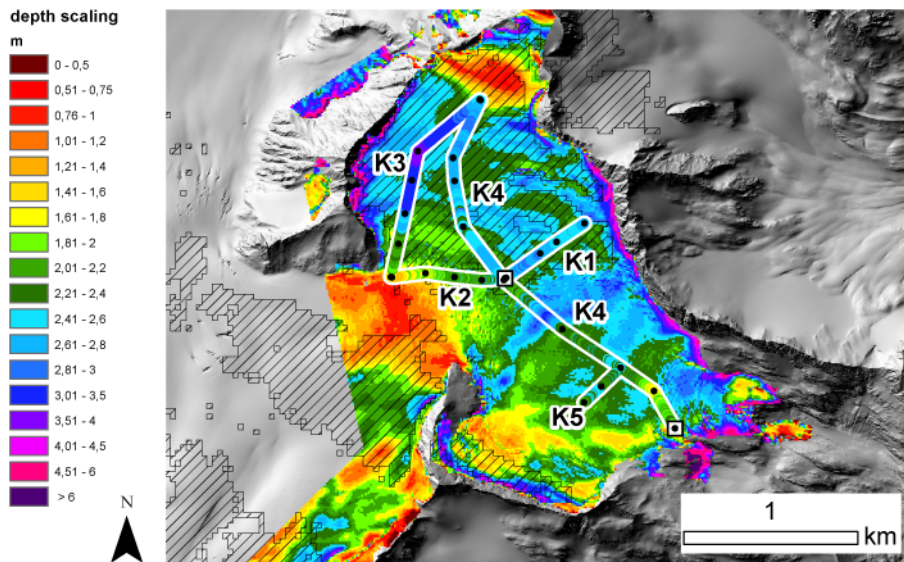
Fig. 6. Spatial distribution of ALS derived surface elevation changes for winter season 2011/2012 and snow depths calculated from GPR measurements along the profiles at Vernagtferner plotted in the same color-scale. Black dots indicate locations of snow depth probing. Locations of snow pits are shown as white squares. Firn areas derived from LANDSAT data are black-striped.
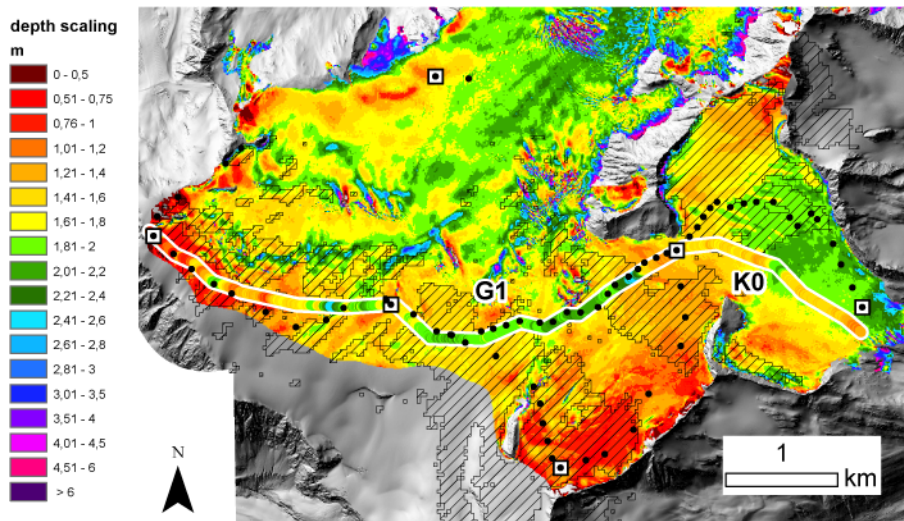
Fig. 7. Spatial distribution of ALS derived surface elevation changes for winter season 2010/2011 and snow depths calculated from GPR measurements along the profiles at Gepatschferner and Kesselwandferner shown in the same color-scale. Black dots indicate locations of snow depth probing. Locations of snow pits are shown as white squares. Firn areas derived from LANDSAT data are black-striped.
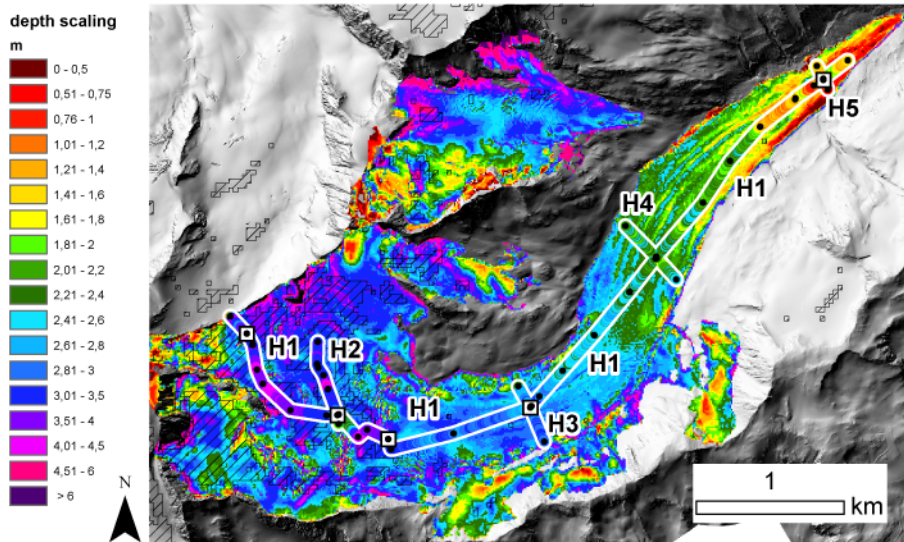
Fig. 8. Spatial distribution of ALS derived surface elevation changes from October 2011 to April 2012 and snow depths calculated from GPR measurements along the profiles at Hintereisferner shown in the same color-scale. Black dots indicate locations of snow depth probing. Locations of snow pits are shown as white squares. Firn areas derived from LANDSAT data are black-striped.

Fig. 9. Spatial distribution of ALS derived surface elevation changes from October 2011 to May 2012 and snow depths calculated from GPR measurements along the profiles at Kesselwand-ferner shown in the same color-scale. Black dots indicate locations of snow depth probing. Locations of snow pits are shown as white squares. Firn areas derived from LANDSAT data are striped with black lines.
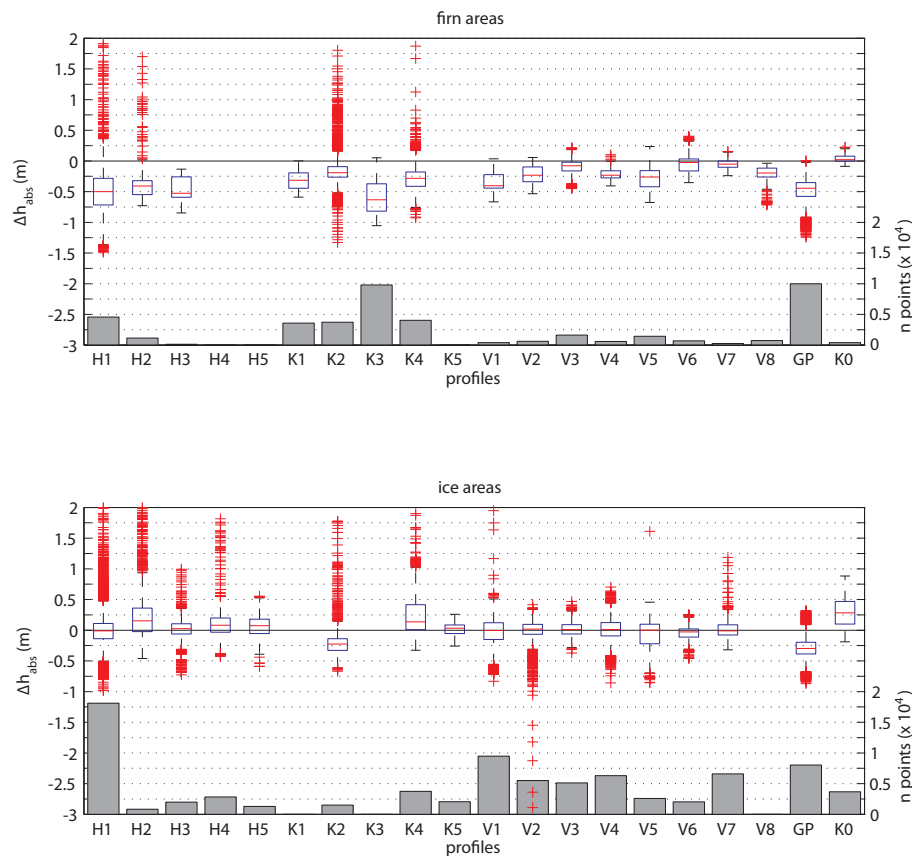
Fig. 10. Box plot of the absolute deviations Δh_{abs} at the profiles for firn areas and ice areas (left scale). Number of points included in the statistics are plotted as bars (right scale).
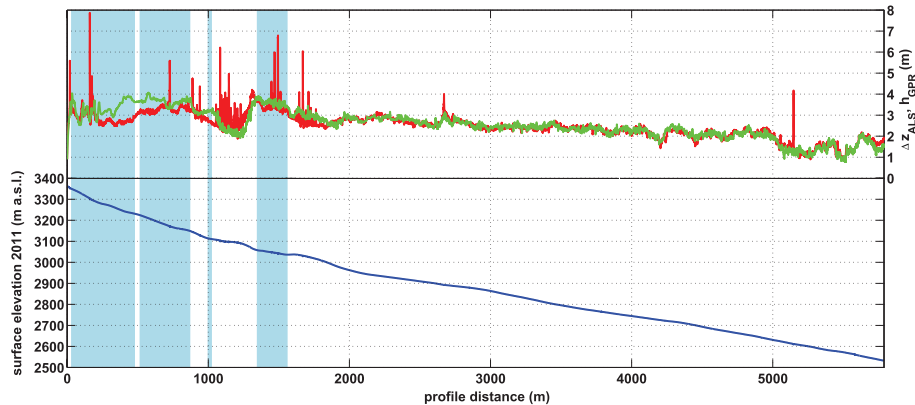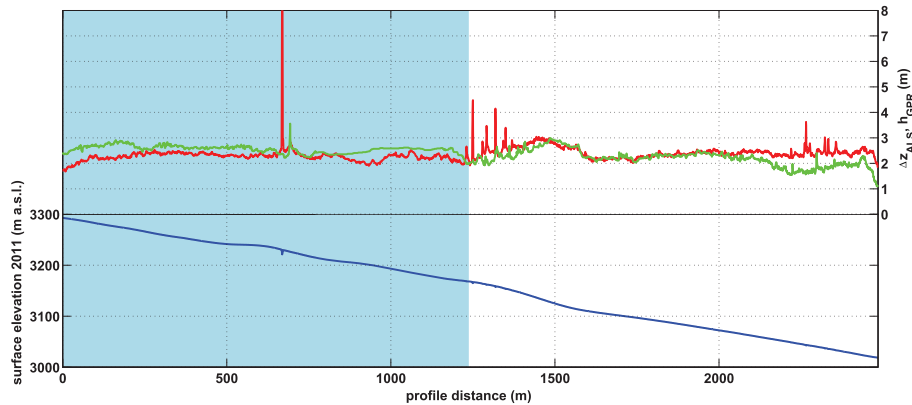
Fig. 11. Elevation of the surface in fall 2011 (blue curve), ALS surface elevation change Δz_{ALS} (red curve) and GPR snow depth h_{GPR} (green curve) along the longitudinal profile H1 at Hintereisferner. The firn areas derived from LANDSAT data are shaded in blue.

Fig. 12. Elevation of the surface in fall 2011 (blue curve), ALS surface elevation change Δz_{ALS} (red curve) and GPR snow depth h_{GPR} (green curve) along the longitudinal profile K4 at Kessel-wandferner. The firn areas derived from LANDSAT data are shaded in blue.